Joint 21st IHPC and 15th IHPS, Melbourne, Australia, February 5-8, 2023

Capillary Jet Loop in direct contact condensation mode used to perform ice protection function of a turboprop composite nacelle intake.

Vincent Dupont[1*], Flavio Accorinti[1], Maxime Henno[2], Patricia Susana Serrano Perez[3], and Francisco Redondo Carracedo[3].

1 Calyos, Charleroi, Belgium
2 SONACA, Gosselie, Belgium
3 Airbus Defence and Space, Getafe, Madrid
**Corresponding author email address: vincent.dupont@calyos-tm.com*

Abstract

In this experimental study a Capillary Jet Loop architecture (CJL-dcc) is proposed to transport the heat from a hot liquid (oil) as heat source to a composite material as coolant surface that is part of the nacelle in a turboprop transport aircraft (as used for Regional and Business Aviation). The application has dual usage, firstly ice protection in cold conditions and cooling of the oil in all conditions. The reduced scale demonstrator tested is a combination of a single capillary loop with a two-phase transport ring (TPR). The ring provides the liquid to the capillary structure and the capillary evaporator induces vapor jets thanks to four injector elements in parallel. The momentum exchange between the high velocity acetone vapor flows and the low velocity of the subcooled liquid ensures both transport and condensation functions before the connecting lines. This paper discusses the design, material and experimental performances of this demonstrator able to transfer 1.24 kW from a 90 x 90 mm² footprint heater. Two different cold sources are investigated with the same injector system and the results are discussed; a tube-in-tube ethylene-glycol water cooled (RS-0/1 demonstrator) and a carbon fiber composite panel (CFRP) with direct melting of an ice volume (RS-2C demonstrator).

Keywords: Anti-icing; Ice protection; Direct Contact Condensation; Injector; Capillary Thermosyphon; Capillary Jet Loop.

1. Introduction

Today, there are numerous heat sources in the nacelles needing to evacuate heat by using heat exchangers typically cooled by external air, inducing additional drag, and making the energy management inefficient. More complexity and weight are added by actuators necessary to control the external air flow.

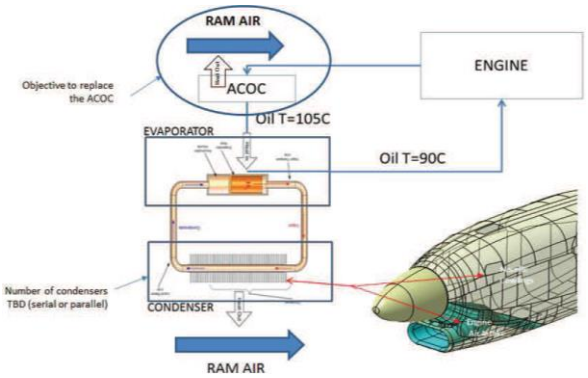

Figure 1. Passive heat recovery concept [1].

For example, the size of traditional heat exchangers could be reduced by extracting part (or all) the heat from the oil used to cool down the engine or the electrical generator and driving it to the nacelle cowlings and/or surfaces where heating is required i.e., ice protected surfaces like engine air intake. In consequence, the nacelle weight and the ram-air required for cooling purposes will also be reduced, resulting in an increased efficiency compared to traditional designs [1].

Two-phase capillary heat transport technologies can be used to recover waste energy from aircraft (sub) systems and/or components. Loop Heat Pipe Ice Protection System have been proposed and successfully tested on several projects [2] but suffer two main limitations. The first one is due to the presence of vapor and liquid in the transport line that makes the system sensitive to the acceleration forces and limits the transport distance and/or the use of ammonia as a working fluid (large latent heat and surface tension). Moreover, if for any reason the design acceleration is exceeded, the capillary evaporator deprimes and the hot source must be cut off before any new heat application, therefore limiting the operability of the aircraft. The second key point is to ensure uniform heat distribution regardless the combination of aircraft attitude, available power, and local acceleration. With parallel connections (embedded tubes inside the CFRP) additional pressure drops are introduced to successfully distribute the flow. But the two-phase pressure gradient is strongly dependent on the vapor quality and the hydrostatic head between channels that make condenser sizing difficult. To overcome these difficulties, the CJL-dcc, patented by Euro Heat Pipes S.A. in Belgium [3], transforms a two-phase flow into a single-phase system [4] to [7].

2. Direct contact condensation with a Capillary Jet Loop (CJL-dcc)

The working principle of the CJL-dcc is presented in the Figure 2 and is described in detail in [3]. This system is a jet pump driven by the vapor flow generated by one or more capillary evaporator. This architecture creates a convenient "thermal bus" and each injector point (10) creates a two-phase flow that can be used to cool or to heat an additional payload ($Q_{HL\,2}$). The momentum exchange between the vapor and the TPR flow induces the fluid motion inside the TPR thanks to the injector elements. The key point of the design in the direct condensation mode is to ensure the complete condensation before reaching the transport line to avoid the presence of vapor at the subcooler inlet and its effects when the TPR is subjected to accelerations.

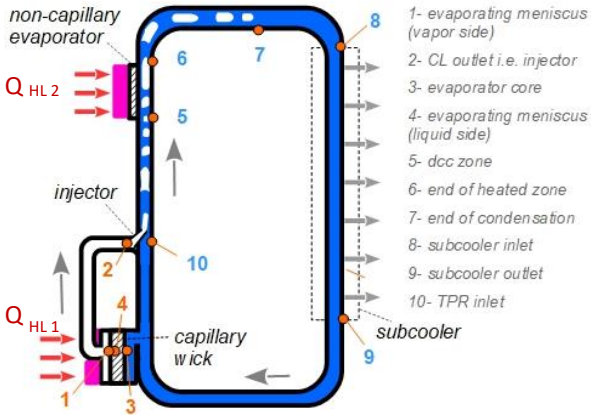

Figure 2. working principle of the CJL-dcc architecture.

3. BISANCE « reduced scale » demonstrator

Due to the advantages mentioned above, the CJL-dcc has been chosen during the preliminary design phase of the BISANCE Cleansky2 project [1] despite a low TRL risk. Based on the Airbus Defence & Space specifications, Calyos and SONACA worked on a collaborative way to propose a full-scale demonstrator design that will be tested in real environment simulator representative of flight dry and icing conditions (RTA Icing Wind Tunnel).

The physics of both hydrodynamics of injection efficiency and in-tube direct condensation heat transfer are poorly documented in the literature, a reduced scale model (TRL-4) is tested to mitigate the design risk and validate the carbon fiber panel manufacturing by SONACA, Belgium. Figure 3 to 5 presents two designs of subcooler tested with acetone as working fluid. The capillary evaporator is a standard Calyos component developed for SiC power electronic cooling. All the parts of the CJL were made with stainless steel except one copper evaporator wall and the aluminum "-dcc box".

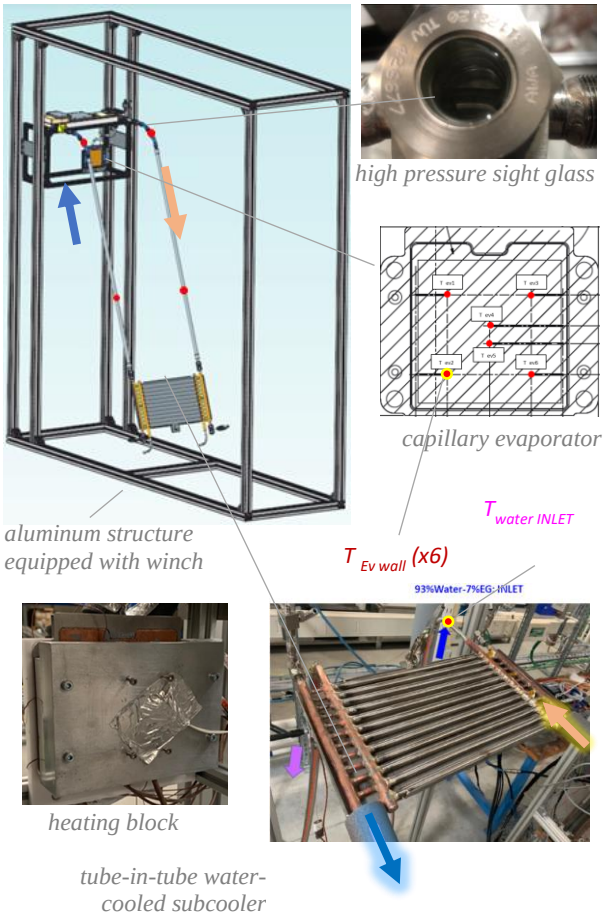

Figure 3. RS-0/1 – overview of the demonstrator equipped with 12 tubes water cooled subcooler.

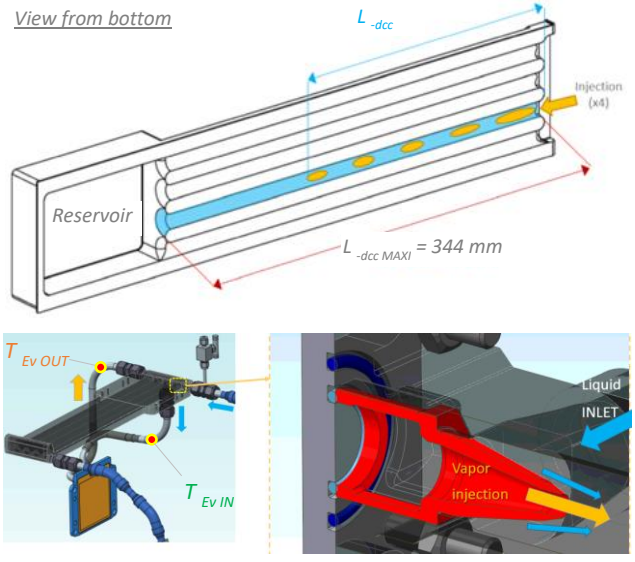

Figure 4. the 3 mm "in-line injector" of the CJL "-dcc box" equipped with four 12mm "-dcc tube".

The capillary loop and the "-dcc box" are the same for RS-0/1 and RS-2C. Thanks to Swagelok connectors, the sight glass, the lines and the subcoolers can be changed to switch from a version to another. Flexibles part are located on the lines to allow relative movement (cf. Figure 14) and to facilitate integration.

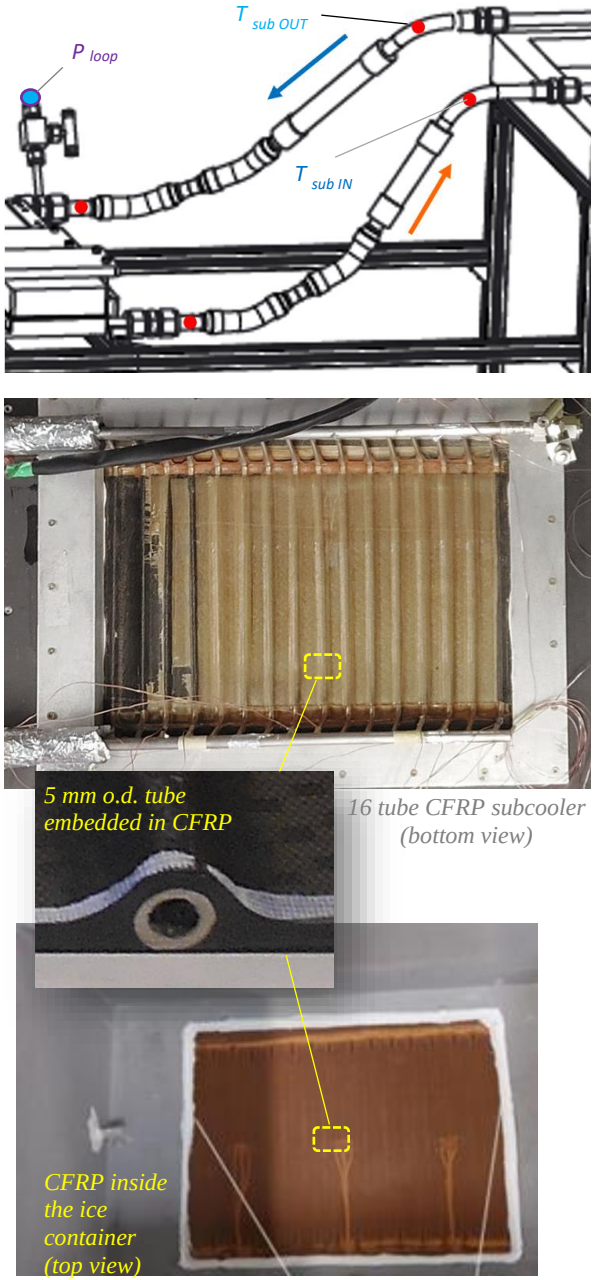

Figure 5. RS-2C – overview of the demonstrator equipped with the 16-tubes CFRP subcooler.

The evaporator performances are evaluated from the temperatures measured, inside the 5 mm thickness wall. The temperature of the 6 thermocouples (TC1 to 6) - bonded inside a 1.2 mm width groove - are averaged to determine $T_{Ev\ wall}$ with an uncertainty of +/-0.3K. The other thermocouples are located outside the tube of the system. The absolute system pressure is measured at the inlet of the "-dcc box" (cf Figure 5) with an absolute pressure transducer Keller PAA-33X, 0-10 bars pressure transducer with an accuracy of 0.10% EM i.e. +/-10 mbar, on the measurement range This pressure is used to determine the saturation temperature $T_{sat}(P_{loop})$ from the NIST Refprop data for acetone. The heating element is an aluminum block equipped with two heating cartridges that replace the oil heat transfer box (OHTB) used on the full-scale demonstrator. The contact area (thermal grease) is 90 x 90 mm² i.e. 1'460 W gives 18W/cm². The energy balance is much easier with an electrical power supply unit but, at contrary there is no decrease of the power with the increase of the saturation condition inside the CJL. The data acquisition device is a standard Agilent 3472A connected to a PC via an Ethernet connection and a LabVIEW interface.

4. RS-0/1 temperature evolution

The RS-0/1 subcooler is based on twelve 7x0.25mm copper inner grooved tube (IGT) with a pitch of 22mm The IGT active length is 360mm and the 14.0mm internal diameter stainless steel manifold (distributor or collector) include a 19.0mm extra length before Swagelok union. A 0.5mm thick annular counterflow is created around each IGT with massflow of 29.2L/min (Water93%-EG7%) and the maximum coolant temperature difference is lower than 0.7K. Figure 6 gives the typical evolutions of the system for 12 hours test with a 143mm favorable tilt identical to the RS-2C setup.

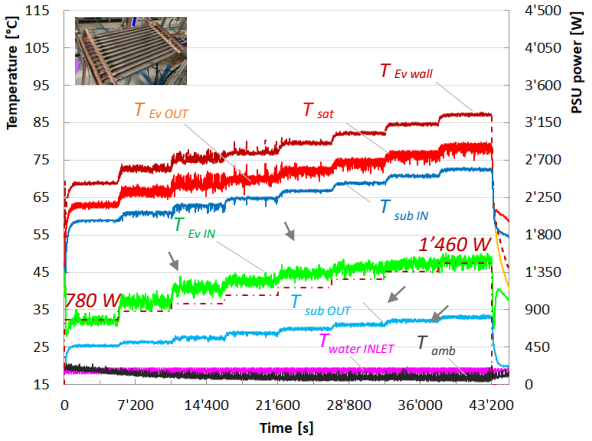

Figure 6. RS-0/1, evolution of the CJL with a favourable tilt h =+143mm.

Some instabilities can be observed around 1kW probably linked to the condensation regime inside

the "-dcc tubes" (cf. Figure 4). The corresponding thermal resistances are analysed in §6.3.

5. Test results for RS-2C demonstrator

The RS-2C subcooler is based on 16 stainless-steel smooth tubes (5x0. 5 mm) with a pitch of 25 mm. The active length is 230 mm and the 10.0mm internal diameter stainless steel manifold (distributor or collector) includes a 78.0 mm extra length before Swagelok union. Half part of the external tubes #1 and #16 are under the silicone sealant (cf. Figure 5) i.e. only 15 tubes are active.

5.1. Molten ice-based energy balance

The ice container is equipped with a water drain located a few centimeters above the level of the composite panel. After a certain time, the water flows by gravity inside a large container located on a Kern DS 30K0.1 industrial scale with an uncertainty of +/- 0.1 gram. Figure 7 shows the measured liquid water mass versus time with the origin corresponding to the first mass measurement. Two phenomena disturb the measurement. First the large ice cubes stick together, and the operator must separate these ice bridges at regular intervals which gives the irregularities on the temperature evolutions on Figures 8). Second, the inlet of the drain is often closed by a floating ice block.

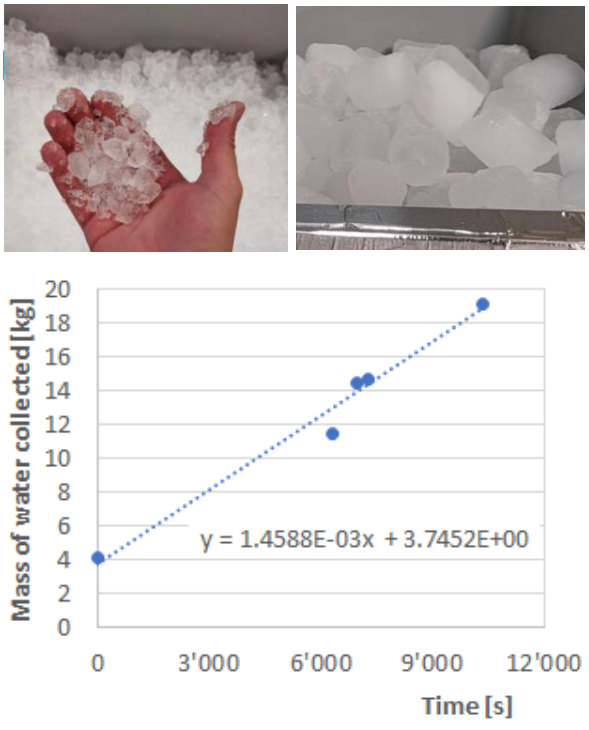

Figure 7. Top: ice grade used during the RS-2C tests. Left: "small" crushed, right: "large" cubes. Bottom: water weight measurement for RUN #2.

The evolution is quasilinear with a melting rate of 1,456 g/s which gives, through an enthalpy balance, a sensible heat power of 52.3W to heat up the ice cubes from -18°C to 0°C (average specific heat of 1'992 J/kg.K) and a fusion power of 486.6W (latent heat of fusion of 333'550J/kg). In total the power estimated from the weight of water is 539W while the average electrical power calculated based on the recordings gives 544W. Thus, the energy balance is respected to within 1% and allows to consider the use of this method at full scale demonstrator level when the heat is extracted from the oil with OHTB's. In this case, the energy balance is more complex in particular because of the variable hydraulic power from the oil pump.

5.2 RS-2C temperature evolution

The ice used can be flakes (ice small) or cylinders of diameter 25 mm and 50 mm in length (ice large). The ice is stored during several days at -18°C before testing and 24kg per run are necessary.

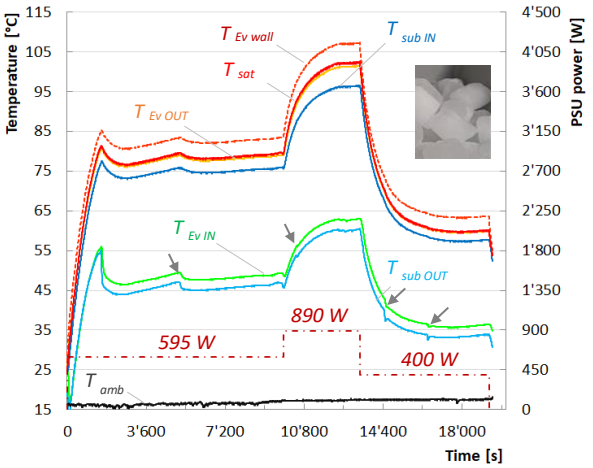

Figure 8. RS-2C, evolution of the CJL temperature during RUN#2 (maximum power).

5.3 Subcooler misdistribution analysis

Figure 9a shows the evolution of the temperature at the outlet of the 16 subcooler tubes (between the CFRP and the collector manifold) as a function of tube position. Tube #0 is T sub IN, tube #17 is T sub OUT and tube #18 is the average value over the 16 outlets. It is demonstrated in §6.3 that for the higher value of massflow the flow remains laminar in the subcooler tubes. In laminar flow, the heat transfer is constant and the measurement of the temperature gradient from inlet to outlet is an indirect measurement of the massflow distribution among the parallel tubes. Figure 9b shows that mass flow varies between -17% and +52% among the 16 subcooler tubes of

the CFRP panel. Better sharing can be obtained with an increase of pressure losses and manufacturing cost of the subcooler with a variable section of the manifolds. Despite a 52% "over massflow" on #2 the corresponding extracted power is only 7.5% above the average. The average value is few degrees below the measured temperature after the collector manifold. This can be explained by the measurement outside the wall (is not exactly the average liquid value). The constant heat transfer coefficient is a too simple assumption and entrance effect and Dean vortices induced by the bends should be considered.

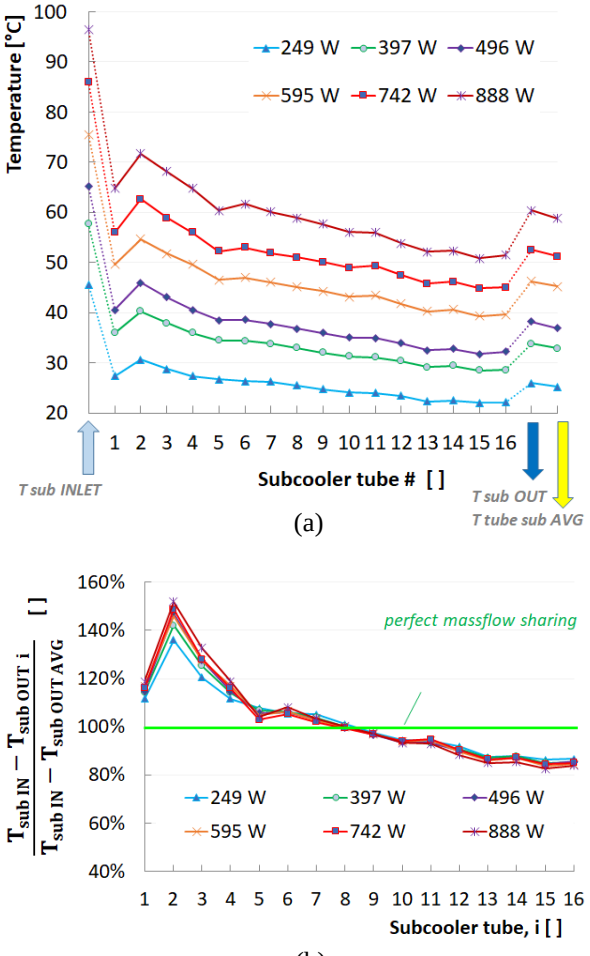

Figure 9. Massflow misdistribution estimation inside the RS-2 composite subcooler: (a) temperature along the manifold for various heat load, (b) deviation from the mean based on the temperature variation of each tube.

6. Performances analysis

6.1. Entrainment ratio γ evaluation

Figure 10 defines the various massflow inside the architecture. One can notice that for a standard LHP (or CPL) there is no additional massflow i.e. γ = 1 (cf. equation 1) inside the TPR.

The relation proposed in [4] for standard in tube condensation is completed and adapted to -dcc mode where the fluid is subcooled at T $_{sub\ IN}$. Considering the subcooling before vaporization, the capillary evaporator enthalpy balance is:

$$Q_{HL} - Q_{losses} = \dot{m}_{vap}\left(\Delta h_{LV} + C_{pL}(T_{sat} - T_{sub\ OUT})\right) \quad (1)$$

where Δh_{LV} refers to the latent heat of vaporization evaluated at saturation, C_{pL} the specific heat of the liquid evaluated at subcooler outlet temperature, $T_{sub\ OUT}$. The entrainment ratio γ is the total massflow inside the TPR divided by the vaporized one:

$$\dot{m}_{TPR} = \gamma\, \dot{m}_{vap} = \dot{m}_{vap} + \dot{m}_{add} \quad (2)$$

The subcooler reject the transferred power by sensible heat variation:

$$Q_{HL} - Q_{losses} = \gamma \dot{m}_{vap}\left(C_{pL}(T_{sub\ IN} - T_{sub\ OUT})\right) \quad (3)$$

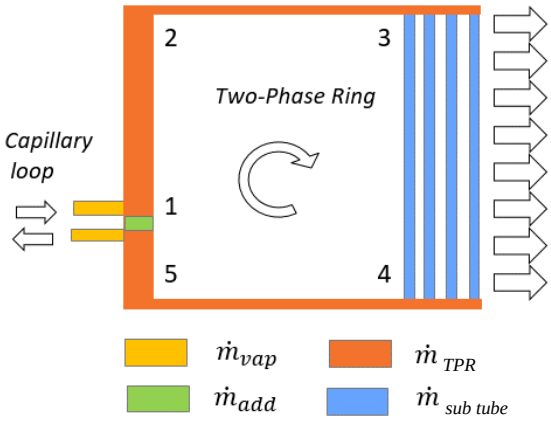

Figure 10. definition of the massflow inside the main hydraulic zones of the CJL-dcc architecture.

Dividing equation 1 by equation 3 gives the relation to evaluate the minimum entrainment ratio (necessary to achieve the -dcc mode) from the measurement of the liquid temperature at inlet (i) and at outlet of a subcooler (ii) and the saturation temperature (iii).

$$\gamma_{-dcc\ min} = \frac{\Delta h_{LV} + C_{pL}(T_{sat} - T_{sub\ OUT})}{Cp_L\, \Delta T_{subcoller}} \quad (4)$$

This value is a thermal constraint mandatory to achieve the complete condensation within the subcooled 344 mm length tubes located before the reservoir, but a higher value can be reached inside

the TPR depending on the hydraulic performances of the TPR. It is possible to simplify equation 4 by considering an ideal system where the subcooler inlet is at saturation:

$$\gamma_{-dcc\,min} \approx \frac{\Delta h_{LV}}{Cp_L\,\Delta T_{subcooler}} + 1 \qquad (5)$$

Equation 4 is used to plot γ versus the power in Figure 11 where the heat losses are estimated to 15% and 1% respectively for the water and the ice container tests. Due to the presence of liquid water in contact with the CFRP, no impact of the type of ice (large or small) has been noticed. The TPR massflow results from the balance between pressure drops and motor terms i.e. injectors momentum and buoyancy forces. Despite a significant difference in the hydraulic network of the RS-0/1 and RS-2C it seems that the two curves overlap perfectly. In subsection 6.3, one can see that the thermal performances of the two types of subcooler, with IGT or smooth tubes, are close. Thus, the overlap of the two curves is more induced by design effect than a general trend but γ seems more driven by the thermal performances than the hydraulic ones. A non-intrusive flowmeter should be used to confirm this analysis.

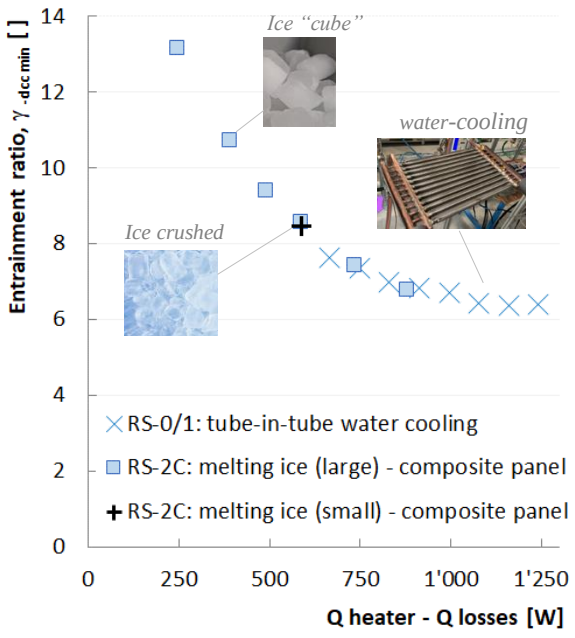

Figure 11. minimum entrainment ratio $\gamma_{-dcc\,min}$ versus power for the two version of the RS-demonstrator. γ is determined from equation 4.

Based on the evaluation of the entrainment ratio γ and the flow distribution over the 16 tubes presented respectively §6.1. and §5.3 it is possible to calculate the liquid velocity of each tube. In our subcooler configuration the maximum mass flow reaches 0.83g/s at tube #2 i.e. the maximum Reynolds number of the inlet of the subcooler tube remains very low, below 15.1, over the entire dataset with melting ice condition which confirms the laminar flow assumption inside the tube 4.0 mm internal diameter smooth tube. In established laminar condition the heat transfer coefficient is independent of the internal massflow (Nu=3.66 for constant temperature boundary condition). Thus, it is a simple justification of the massflow distribution presented in §5.3. In fact, the situation is more complex and entrance effect and Dean vortices induced by the bend should be considered.

6.2. Thermal resistance of the CFRP

The initial goal of the Clean Sky 2 call [1] was to investigate the feasibility and the thermal performance of the carbon fiber panel equipped with embedded hydraulic network. SONACA has developed the Bisance subcooler in collaboration with Calyos to magnify the thermal performances at reasonable cost and weight. In particular, the manufacturing constraint impose limitations in terms of tube diameter, material and pitch.

Calyos performed 2D simulations of the SONACA CFRP stacking. The thermal conductivity of the CFRP is 0.4 W/m.K transverse and 15 W/m.K in-plane. The stainless-steel tube, the adhesive and the bronze mesh are at, respectively, 16, 0.2 and 42 W/m.K. The number and the thicknesses of the various layers are SONACA proprietary information's and cannot be disclosed in the present communication. Figure 12 gives a view of the complex conductivity field due to the specific shape of the CFRP fabric.

The freeFEM++ open-source software has been used with a structured mesh approach with a typical cell size of 0.1 mm. The main result of these calculations is that the transmittance value of the CFRP including the 5x0.5mm stainless steel tube is estimated to 162 W/m²K (with respect to the external panel area) and is not sensitive to the value of internal heat transfer coefficient.

This transmittance can be used to determine the local heat transferred to the ice along each subcooler tube. Due to the fin efficiency effect of the stacking, the heat flux is 67% higher in front of the tube in comparison to the center of the pitch (Figure 12). Considering an area of 900 cm² in contact with the ice (15 tubes) the conductive thermal resistance is 68.6 K/kW. It is a rough approximation because it does not consider the variation of the liquid temperature inside the subcooler (a log min temperature approach should be used for example).

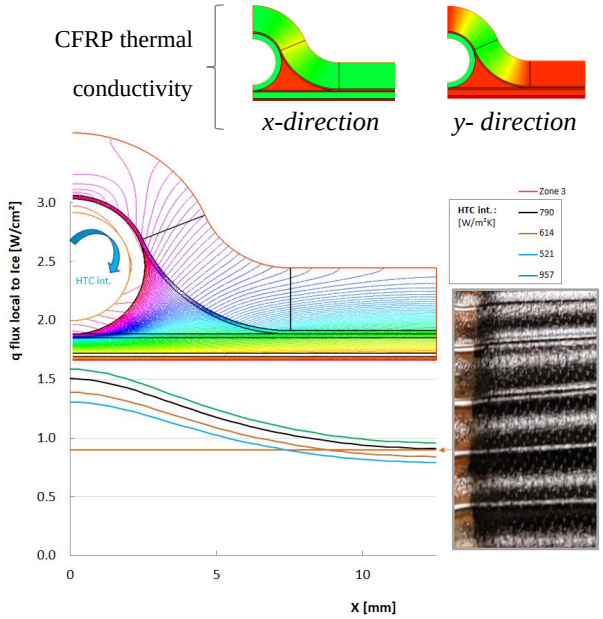

Figure 12. 2D simulations of the elementary section for the composite stacking. The heat flux versus position is given for various internal heat transfer coefficient with T fluid = 100°C and T ext. panel = 0°C (melting ice condition).

6.3. Thermal resistance synthesis

Figure 13 shows the evolution of the various thermal resistances inside the system from the evaporation copper wall to the coolant inlet flow.

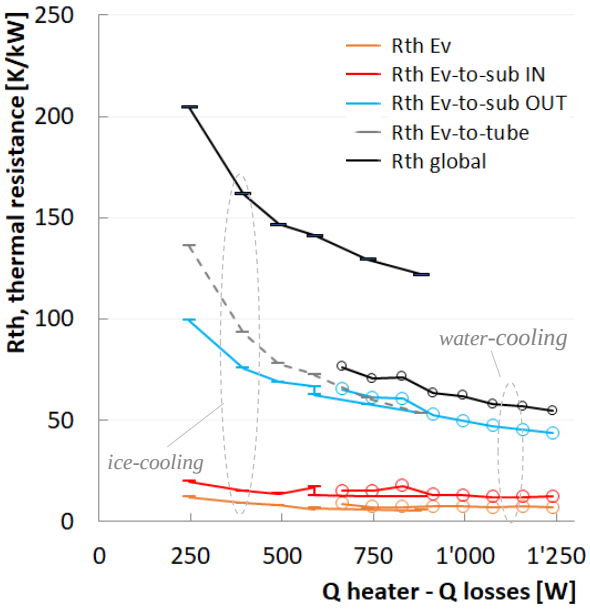

Figure 13. Thermal resistance sharing during the tube-in-tube water cooling and ice container tests.

The sum of the vaporization and the direct contact condensation thermal resistances is lower than 17 K/kW i.e. from 20 to 25% of the total thermal resistance for the tube-in-tube water cooling and from 9 to 12% for the melting ice on CFRP. The condensation takes place inside 344 mm long 12mm i.d. "-dcc tubes" located directly after the 4 injectors. By design the vapor is not allowed to flow to the subcooler. This type of condensation is efficient, and the number of injectors in parallel can be scaled up to address higher heat load values.

The efficiency of the subcooler tubes is the bottle neck of the RS-2C water-cooled version and because the flow remains laminar multiport approach must be privileged.

The transmittance of the CFRP induces an additional thermal resistance of the same order than the liquid heat transfer coefficient and clearly limits the transferred power in the RS-0/1 configuration.

Thus, it is not yet possible to use the tested panel for anti-icing purpose. Improvements are necessary to decrease the necessary minimum oil temperature. It is possible to gain 15% of exchange surface by reducing the thickness of stainless-steel tubes and / or by splitting the flow with a multiport approach

6.4. Tilt impact

Figure 14 shows the impact of the tilt on the TPR entrainment ratio evaluated from equation 4 and also the buoyancy pressure induced by the liquid density difference between the "hot" riser and the "cold" downcomer at 1'271 W.

The entrainment ratio γ inside the TPR decreases with the heat load and ranges from 6.4 to 13.1 in the present conditions. Increasing the heat load induces an increase of the saturation condition (cf. Figure 6 and 8) that leads to lower velocity at injector outlet. Thus, the contribution of the injector is too low at high temperature with respect to the buoyancy forces and it is necessary to operate lower saturation condition and/or to adapt the section of the injector.

CFD simulation work is underway to increase γ parameter value through an optimization of the injector zone and is presented in a sister paper [8].

4. Conclusions and perspectives

The tests carried out on this demonstrator made prove that it is possible to functionalize carbon fiber panels (CFRP) by including metal tubes to evacuate heat from a passive two-phase loop and to perform anti-icing function.

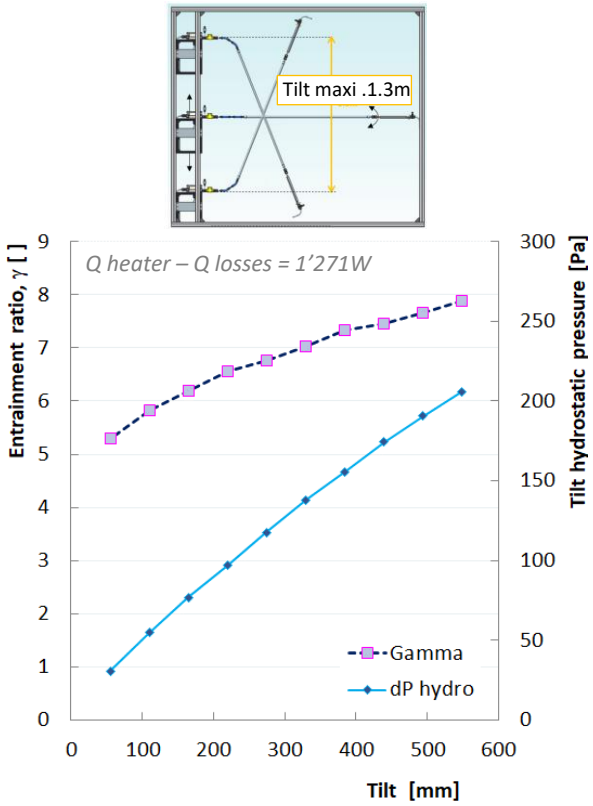

Figure 14. Influence of the location of the subcooler position with respect to the injectors.

During the trade-off phase the direct condensation Capillary Jet Loop appear to be the most promising technology. The main advantages are a better resistance to accelerations and ease of distribution of the liquid flow on a complex volumetric heat exchanger like a turbomachine air intake.

The system was tested by melting a volume of ice to mimic the final demonstrator configuration and its operating range has been extended thanks to a tube-in-tube water exchanger but keeping the thermal performance equivalent to that of the CFRP subcooler.

It has been shown that the Capillary evaporator equipped with 4 injectors can transport 1.46 kW in the full-size demonstrator conditions. The condensation takes place inside 344 mm long "-dcc tubes" located directly after the 4 injectors. By design of the "-dcc box" the vapor cannot flow to the subcooler. The part of vaporization and condensation contribution to thermal resistance ranges from 20 to 25% for the tube-in-tube water cooling and from 9 to 12% for the melting ice on CFRP.

The constraints of the CFRP manufacturing process as well as the thermomechanical limits dictated the diameter, the material and the pitch of the integrated tubes limiting the transmittance to 160 W/m.K.

TRL 4 level is reached with this reduced scale demonstrator and TRL-5 tests on the full size protype are scheduled in the RTA main Icing Wind Tunnel in Vienna (Austria) for the second week of February 2023.

Acknowledgement

The Bisance project has received funding from the Clean Sky 2 Joint Undertaking under the European Union's Horizon 2020 research and innovation programme under grant agreement No 865113. This publication reflects only the author's views, and the JU is not responsible for any use that may be made of the information it contains.

References

[1] Biphasic Heat Transport Integration for Efficient Heat Exchange within Composite materials Nacelle. JTI-CS2-2018-CFP09-AIR-02-69. Cleansky Call for proposal.

[2] Q. Su, S. Chang, Y. Zhao, H. Zheng and C. Dang, A review of loop heat pipes for aircraft anti-icing applications. Applied Thermal Engineering, 2018. 130: pp. 528-540.

[3] Patent FR3032027. 2015.

[4] V. Dupont., B. Paran, S. Van Oost, and C. Billet. Capillary Jet Loop in 19th International Heat Pipe Conference. 2018. Pisa, Italy.

[5] V. Dupont and O. de Laet. Two-phase thermal bus for multiple heat sources passive cooling. 2019. 1st joint International Forum Automotive Aerodynamics & Thermal Management. Manchester, UK.

[6] L. Araneo, R. Clavenna, R. Boubaker, V. Dupont. Performance analysis and simplified modelling of a capillary jet loop heat pipe.2021. Applied Thermal Engineering. Volume 197, 117407.

[7] R. Clavenna, L. Araneo, V. Dupont, R. Boubaker. Capillary Jet Loop performance in parabolic flight. Applied Thermal Engineering, 2022. 217: 119221.

[8] C. Braga Vieira, T. Nicolle, F. Accorinti, O. de Ghelin, C. Goffaux and V. Dupont. Computational simulation of a vapor jet into a subcooled flow inside a capillary jet loop system operating in direct condensation mode in Joint 21st IHPC and 15th IHPS. 2023. Melbourne, Australia.